

Electron Energy Distributions in H II Regions and Planetary Nebulae: κ -Distributions Do Not Apply

B. T. Draine and C. D. Kreisch

Princeton University Observatory, Peyton Hall, Princeton, NJ 08544-1001, USA;
draine@astro.princeton.edu, ckreisch@astro.princeton.edu

ABSTRACT

Some authors have proposed that electron energy distributions in H II regions and planetary nebulae may be significantly nonthermal, and κ -distributions have been suggested as being appropriate. Here it is demonstrated that the electron energy distribution function is extremely close to a Maxwellian up to electron kinetic energies ~ 13 eV in H II regions, and up to ~ 16 eV in planetary nebulae: κ -distributions are inappropriate. The small departures from a Maxwellian have negligible effects on line ratios. When observed line ratios in H II regions deviate from models with a single electron temperature, it must arise from spatial variations in electron temperature, rather than local deviations from a Maxwellian.

Subject headings: atomic processes — plasmas — ISM: general — H II regions — planetary nebulae: general

1. Introduction

Observed ratios of collisionally-excited emission lines from H II regions and planetary nebulae in some cases depart from the predictions for a plasma with thermally-distributed electrons with a single electron temperature T_e . Discrepancies are also found when comparing T_e determined from ratios of collisionally-excited lines (e.g., [O III]4364/[O III]5008) with T_e estimated from the Balmer or Paschen discontinuities in hydrogen recombination spectra. Finally, abundances estimated from the faint recombination lines of heavy elements often differ substantially from abundances estimated from collisionally-excited lines.

Peimbert (1967) proposed that the observed line ratios in H II regions are due to spatial variations in T_e within the photoionized gas – which Peimbert referred to as “temperature fluctuations” – and line ratios are sometimes interpreted within this framework (e.g., Louise & Monnet 1969; Liu & Danziger 1993; Kingdon & Ferland 1995; Gruenwald & Viegas 1995; Perez 1997; Kingdon & Ferland 1998; Binette & Luridiana 2000; O’Dell et al. 2003; Zhang et al. 2007; Oliveira et al. 2008). Esteban (2002) reviewed arguments for and against the existence of such temperature variations within ionized nebulae. Binette et al. (2012) claimed that observed line ratios in H II regions could

not be accounted for by temperature inhomogeneities, and argued that the observed line ratios required either unusual heating mechanisms (e.g., shock waves), metallicity inhomogeneities, or electron energy distributions given by the κ -distribution instead of the Maxwell-Boltzmann distribution.

Some authors have proposed that the energy distribution functions may *locally* depart from a Maxwellian distribution. Giammanco & Beckman (2005) proposed that ionization by cosmic rays could be responsible for non-Maxwellian electron energy distributions. Nicholls et al. (2012) have argued that the electron energies obey a κ -distribution, and Nicholls et al. (2013), Dopita et al. (2013), and Mendoza & Bautista (2014) have calculated emission line ratios assuming the electron energies to be κ -distributed. Zhang et al. (2014) discussed κ -distributed electrons in planetary nebulae.

The κ -distribution has been found to describe the distribution of electron energies in interplanetary plasmas (Pierrard & Lazar 2010), where the low densities of the solar wind are insufficient to establish a thermal distribution given the high temperatures and short time scales associated with flow from the Sun to the Earth’s orbit.

By contrast, it had generally been assumed that for conditions in H II regions, elastic scattering is fast enough that the electron energy distribution should be very close to a Maxwell-Boltzmann distribution (Spitzer 1941, 1968). Ferland et al. (2016) estimated the time scales and distances on which suprathermal electrons in an H II region would be thermalized, and argued that the speed of thermalization suggested that it was unlikely that such electrons could affect the collisionally-excited forbidden lines, but noted that there did not appear to be any numerical calculations examining this in detail.

Because of the recent proposals that electron energy distributions in H II regions may be significantly non-Maxwellian, we revisit this problem here. From first principles, we explicitly solve for the steady-state distribution of electron energies in a partially-ionized plasma where heating of the plasma is done by injection of energetic photoelectrons resulting from photoionization of H atoms that have been formed by radiative recombination, and where electron cooling is accomplished by various processes, including radiative recombination, free-free emission, and collisional excitation of species such as O III and S III.

We show that the electron energy distribution relaxes rapidly to a steady-state distribution that is very close to a Maxwellian. Slight departures from a Maxwellian do occur, but are far too small to noticeably affect observed emission line ratios.

The paper is organized as follows. The statistical problem for the steady-state case is formulated in Section 2. The atomic processes are reviewed in Section 3: the Coulomb scattering responsible for thermalization, radiative recombination of hydrogen followed by injection of photoelectrons, and cooling by free-free emission and collisional excitation of ions.

In Section 4 we present the steady-state solution for the electron energy distribution in an

H II region with a representative spectrum of photoelectrons. The steady-state solutions are shown to be extremely close to a Maxwell-Boltzmann distribution, with only small departures at very suprathermal energies. The κ -distribution does *not* describe the electron energy distribution.

In Section 5 we study the time evolution of an electron distribution starting from an initial distribution that is far from thermal; relaxation to a near-thermal distribution takes place extremely rapidly. For conditions in the Orion Nebula, thermal relaxation is accomplished in ~ 30 sec. In Section 6 we model the electron energy distribution in a prototypical planetary nebulae, photoionized by radiation from a 10^5 K star.

We conclude that electron energy distributions in H II regions and planetary nebulae will be locally very close to Maxwell-Boltzmann, except for a high energy tail containing only a very small fraction of the electrons. There is no basis for using the κ -distribution to describe the distribution of electron energies in H II regions and planetary nebulae.

Certain technical details concerning the treatment of elastic scattering are presented in the Appendix.

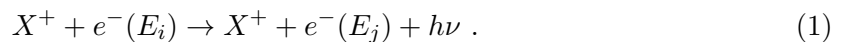
2. Formulation of the Problem

To study the distribution of electron energies, we define N electron energy “bins” $j = 1, \dots, N$, where bin j includes kinetic energies $(j - 1)\delta E < E < j\delta E$, where $\delta E \equiv E_{\max}/N$.

Let n_e be the electron density, and let P_j be the fraction of the electrons having energies in bin j . Let n_X be the number density of other species X present. An electron in bin j can be scattered to a bin $k \neq j$ by elastic scattering off electrons or ions, or by inelastic scattering by atoms or ions, where some of the initial energy E_j goes into excitation of the atom or ion. Scattering of the electron by ions can result in energy loss by bremsstrahlung. Radiative recombination can remove the electron from bin j , and photoionization will inject new electrons into the energy distribution.

Transition rates for a number of distinct processes are required:

- $A_{kij}P_j$ = probability per unit time that an electron with energy E_i will gain energy E_k from an electron with energy E_j , becoming an electron with energy $E_i + E_k$. The electron with energy E_j becomes an electron with energy $E_j - E_k$.
- B_{ji} = probability per unit time that an electron with energy E_i will radiate a continuum photon $h\nu = E_i - E_j$ as a result of free-free scattering by an ion X^+ :



- C_{ji} = probability per unit time of inelastic scattering of an electron of energy E_i by one of the species in the gas (e.g., S II, N II, O III) with energy loss $E_i - E_j$ corresponding to excitation of

the target species. The transition matrix C_{ji} should include all important inelastic excitation channels.

- R_i = probability per unit time that an electron with energy E_i will undergo radiative recombination

$$X^+ + e^-(E_i) \rightarrow X + h\nu . \quad (2)$$

The only important species to consider for X are H and He. We assume that radiative recombination is balanced by photoionization

$$X + h\nu \rightarrow X^+ + e^-(E) , \quad (3)$$

where $E = h\nu - I_X$. Let ϕ_j be the probability that the photoionization event has $E \in [E_j - \delta E/2, E_j + \delta E/2]$. The assumption that recombination is instantaneously balanced by photoionization is not exact for time-dependent calculations, but remains a good approximation if the density of ionizing photons is high so that the time for photoionization is short, and the neutral fraction is very small (i.e., high values of the “ionization parameter”).

We assume that E_{\max} is large enough that transitions to and from electron energies $E > E_{\max}$ can be neglected, and $\sum_{j=1}^N P_j = 1$. E_{\max} should be large enough that photoionization events producing photoelectrons with $E > E_{\max}$ can be neglected. This corresponds to assuming that the ionizing spectrum does not extend beyond $h\nu = I_H + E_{\max}$. For photoionization by massive stars, we will typically take $E_{\max} = 25$ eV. This value of E_{\max} allows for injection of photoelectrons resulting from photoionization by photons up to $h\nu = I_H + E_{\max} = 38.6$ eV, which includes over 99% of the ionizing radiation from a star with $T_\star = 35000$ K (spectral type O8V). To study the electron energy distribution for conditions in planetary nebulae, we set $E_{\max} = 75$ eV, allowing for photoionization of H by photons up to $h\nu = 88.6$ eV, which includes over 99% of the ionizing radiation for a $T_\star = 10^5$ K blackbody spectrum.

For every i , we have

$$\begin{aligned} \frac{dP_i}{dt} = & \left(\sum_{j=1}^N R_j P_j \right) \phi_i - R_i P_i + \sum_{j=i+1}^N (B_{ij} + C_{ij}) P_j - \sum_{j=1}^{i-1} (B_{ji} + C_{ji}) P_i \\ & + \sum_{j=1}^{i-1} \sum_{k=i-j+1}^N A_{i-j,j,k} P_j P_k + \sum_{k=i+1}^N \sum_{j=1}^{N-(k-i)} A_{k-i,j,k} P_j P_k \\ & - \sum_{j=1}^{N-i} \sum_{k=j+1}^N A_{j,i,k} P_i P_k - \sum_{j=1}^{i-1} \sum_{k=1}^{N-j} A_{j,k,i} P_k P_i . \end{aligned} \quad (4)$$

The physics is contained in A_{ijk} , B_{ij} , C_{ij} , R_i , and ϕ_i .

3. Physical Processes

3.1. Elastic Scattering

Elastic scattering is the fastest and most important process, and accurate calculation of the $O(N^3)$ nonzero elements of A_{ijk} is challenging. For the Coulomb interaction, large impact parameter weak scattering events make the dominant contribution to energy transfer. These weak-scattering events must be treated with some care. The key length scale is the plasma Debye length

$$L_{\text{Debye}} = 690 \left(\frac{T_e}{10^4 \text{ K}} \right)^{1/2} \left(\frac{n_e}{\text{cm}^{-3}} \right)^{-1/2} \text{ cm} . \quad (5)$$

On scales short compared to L_{Debye} the electrons and ions are located randomly, but on longer length scales electrons and ions are correlated, leading to screening.

In the center-of-mass frame, the electron-electron scattering problem is entirely characterized by the center-of-mass energy and the impact parameter b . For impact parameter $b < L_{\text{Debye}}$ we assume that screening effects can be neglected and the interaction is described by classical 2-body Rutherford scattering, with differential scattering cross section (e.g. Landau & Lifshitz 1976)

$$\frac{d\sigma}{d\Omega} = \left(\frac{e^2}{4E_{\text{CM}}} \right)^2 \frac{1}{\sin^4(\theta/2)} , \quad (6)$$

where θ is the scattering angle in the center-of-mass frame, and E_{CM} is the center-of-mass energy. For $b > L_{\text{Debye}}$, we assume that screening is highly effective, and these events will be neglected entirely. Our approximations will overestimate the contribution of scattering events with impact parameters $0.5L_{\text{Debye}} \lesssim b < L_{\text{Debye}}$, while underestimating (by entirely neglecting) the contribution of scattering events with $b > L_{\text{Debye}}$.

Consider scattering between electrons with energy E_j and E_k . For $i > 1$ we take A_{ijk} to be defined so that $A_{ijk}E_i$ is the correct rate of energy transfer in scattering events where the electron with initial energy E_j scatters into states with final energy in $[E_{i+j} - \frac{\delta E}{2}, E_{i+j} + \frac{\delta E}{2}]$. For chosen E_j and E_k , computation of A_{ijk} requires determining the rate of collisions such that the electron with initial energy E_j emerges with kinetic energy increased by $\Delta E \in [i - \frac{1}{2}, i + \frac{1}{2}]\delta E$.

The smallest energy transfer events must be treated carefully, because they dominate the total loss rate. For A_{1jk} and $k > j$ we include all events where electron k loses energy with $|\Delta E| < \frac{3}{2}\delta E$.

We explicitly calculate scattering rates A_{ijk} where $E_k > E_j$ and particle j gains energy from particle k . For $j \leq k$ we obtain the A_{ijk} using detailed balance (see Appendix D).

Further details of our treatment of elastic scattering are provided in Appendices A–D. Figure 1 shows the net rate of energy change dE/dt due to elastic scattering only,

$$\left(\frac{dE}{dt} \right)_i = \sum_{j=1}^N \sum_{k=1}^N (A_{kij} - A_{kji}) P_j E_k \quad (7)$$

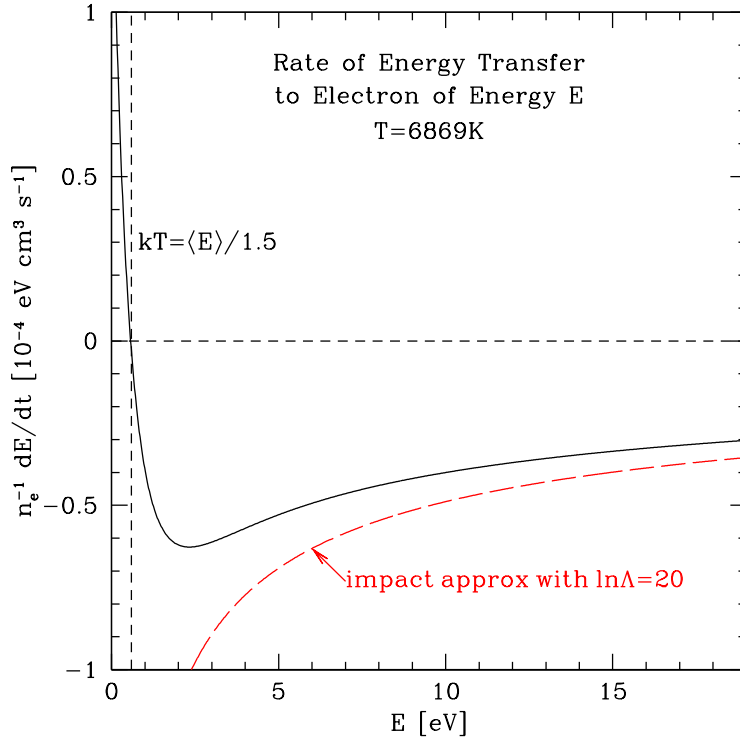


Fig. 1.— Average rate of energy gain or loss for an electron of energy E due to elastic scattering in a thermal plasma of temperature $T = 6869$ K, the temperature corresponding to thermal equilibrium for the conditions considered below.

as a function of electron energy E_i , for a thermal distribution P_j . As expected, dE/dt is zero for $E = \langle E \rangle = 1.5k_B T$, where k_B is Boltzmann’s constant; lower energy electrons systematically gain energy, while higher energy electrons on the average lose energy to their neighbors. The broken line in Figure 1 shows the rate of energy loss for an electron moving through a zero temperature plasma, calculated using the impact approximation (e.g., §2.2.1 of Draine 2011), which should be valid for energies $E \gg \langle E \rangle$:

$$\frac{dE}{dt} = -\frac{4\pi n_e e^4}{(2m_e E)^{1/2}} \ln \Lambda, \quad (8)$$

where $\ln \Lambda \approx 20$ is the usual Coulomb logarithm. For $E \gtrsim 10$ eV our calculated rate of net energy change is in fairly good agreement with Eq. (8).

3.2. Radiative Recombination and Injection of Photoelectrons

We assume “case B” recombination, neglecting radiative recombination directly to the ground state. If the case B radiative recombination rate coefficient in a thermal plasma is approximated by a power-law $\alpha_B \approx 2.59 \times 10^{-13} T_4^{-0.81} \text{ cm}^3 \text{ s}^{-1}$ (see, e.g., Draine 2011), then it follows that the

rate coefficient for recombination of an electron of energy E varies as

$$\alpha(E) = 1.55 \times 10^{-13} \left(\frac{E}{\text{eV}} \right)^{-1.31} \text{ cm}^3 \text{ s}^{-1} . \quad (9)$$

Thus,

$$R_i = 1.55 \times 10^{-13} \left(\frac{E_i}{\text{eV}} \right)^{-1.31} \text{ cm}^3 \text{ s}^{-1} \times n(\text{H}^+) . \quad (10)$$

Recombination preferentially removes low-energy electrons.

In the steady-state, every recombination is balanced by a photoionization. The energy distribution ϕ_i of the photoelectrons is determined by the spectrum of the absorbed photons. This will vary with distance from the exciting star, with softer photons being preferentially absorbed near the star, hardening the spectrum with increasing distance from the star. Near the star the photoionization rate is dominated by the stellar photons with energies just above I_{H} . The photon spectrum hardens as one moves away from the star, and near the outer edge of the H II region the ionizing spectrum is hardest, and the mean photoelectron energy is highest. If every ionizing photon is absorbed somewhere, then the overall average spectrum will be that of the ionizing photons emitted by the star. For simplicity, we approximate the stellar spectrum by a blackbody of temperature T_{\star} , and assume all photoionizations come from hydrogen. Therefore, for stellar temperature T_{\star} , we approximate the spectrum of photoelectrons by the average spectrum

$$\phi_i = \frac{(I_{\text{H}} + E_i)^2 / [e^{(I_{\text{H}} + E_i)/k_{\text{B}}T_{\star}} - 1]}{\sum_{j=1}^N (I_{\text{H}} + E_j)^2 / [e^{(I_{\text{H}} + E_j)/k_{\text{B}}T_{\star}} - 1]} . \quad (11)$$

If the exciting star is hot enough to appreciably ionize He, then helium ionization and recombination will also occur. On the one hand, this provides an additional heating mechanism; on the other hand, because of the higher ionization threshold, the photoelectrons will be less energetic. For simplicity, we will ignore both photoionization and recombination of helium. With $n(\text{He}^+)/n(\text{H}^+) \approx 0.1$, we are thereby underestimating the overall photoelectric heating rate by perhaps $\sim 10\%$ for a plasma where the helium is predominantly He II.

We adopt $T_{\star} = 35000 \text{ K}$ to characterize an ionizing spectrum similar to a star of spectral type O8V, approximately representative of the spectrum of stars powering typical H II regions in star-forming galaxies.¹ For $T_{\star} = 35000 \text{ K}$, the distribution (11) has a mean photoelectron energy

$$\langle E_{\text{pe}} \rangle = \sum_{i=1}^N \phi_i E_i \approx 4.22 \text{ eV} . \quad (12)$$

For $T_{\star} = 1.0 \times 10^5 \text{ K}$, $\langle E_{\text{pe}} \rangle = 15.83 \text{ eV}$.

¹E.g., $\theta^1\text{Ori C}$ (O7V) and $\theta^1\text{Ori D}$ (O9.5V) in the Orion Nebula (O'Dell 2001), with effective temperatures $T_{\text{eff}} = 37000 \text{ K}$ and 32000 K .

3.3. Free-Free Radiation

As a simple approximation, we assume that an electron of energy E_i scattering off singly-charged ions with density n_e radiates with power per unit frequency

$$p_\nu(E_i) = A_0 h n_e \left(\frac{\text{eV}}{E_i} \right)^{1/2} \quad h\nu < E_i \quad (13)$$

$$= 0 \quad h\nu > E_j, \quad (14)$$

where A_0 is a constant. With this assumption, a thermal distribution would have

$$\frac{4\pi j_\nu}{n_e} = \frac{2}{\sqrt{\pi}} A_0 h n_e \left(\frac{\text{eV}}{k_B T} \right)^{1/2} e^{-h\nu/k_B T}, \quad (15)$$

and total radiated power per electron

$$\frac{\Lambda}{n_e} = \frac{2}{\sqrt{\pi}} A_0 n_e (\text{eV } k_B T)^{1/2} \quad (16)$$

$$= 1.91 \times 10^{-25} \left(\frac{n_e}{\text{cm}^{-3}} \right) \left(\frac{T}{10^4 \text{K}} \right)^{1/2} \text{erg s}^{-1}, \quad (17)$$

for $A_0 = 1.108 \times 10^{-13} \text{cm}^3 \text{s}^{-1}$. This corresponds to assuming a constant Gaunt factor $g_{\text{ff}} = 1.34$, which is the frequency-averaged value near $T = 10^4 \text{K}$. [see, e.g., Eq. (10.10) in Draine (2011)].

The probability per unit time of an electron of energy E_i making a transition to bin $j < i$ is related to the radiated power by

$$(E_i - E_j) B_{ji} = p_\nu(E_i) \frac{\delta E}{h}. \quad (18)$$

Thus, the probability per time of a transition resulting from emission of a photon is

$$B_{ji} = A_0 n_e \left(\frac{\text{eV}}{E_i} \right)^{1/2} \frac{\delta E}{(E_i - E_j)} \quad (19)$$

$$= \frac{1.108 \times 10^{-13} \text{s}^{-1}}{(E_i/\text{eV})^{1/2}} \left(\frac{n_e}{\text{cm}^{-3}} \right) \frac{1}{(i - j)} \quad \text{for } i > j. \quad (20)$$

3.4. Collisional Excitation of Ions

Electrons can undergo inelastic scattering with electron kinetic energy going into electronic excitation of abundant ions such as N II, S II, and O III. In Table 1 we list the transitions included here, and the sources of inelastic cross sections.

Consider excitation of an ion X from level ℓ to level u , requiring excitation energy $\Delta E_{u\ell}$. The cross section for excitation is expressed in terms of a dimensionless energy-dependent collision strength $\Omega(E)$:

$$\sigma(E_i) = \pi a_0^2 \frac{I_{\text{H}}}{E_i} \frac{\Omega_{\ell \rightarrow u}(E_i)}{g_\ell} \quad \text{for } E_i > \Delta E_{u\ell} \quad (21)$$

Table 1: Collisional Excitation Channels

X	ℓ	u	$(E_u - E_\ell)/hc$ (cm^{-1})	$(E_u - E_\ell)$ (eV)	reference
N II	3P_0	3P_1	48.7	0.00604	Tayal (2011)
C II	$^2P_{1/2}^o$	$^2P_{3/2}^o$	63.4	0.00786	Liang et al. (2012)
O III	3P_0	3P_1	113.2	0.0140	Tayal & Zatsarinny (2017)
N II	3P_0	3P_2	130.8	0.0162	Tayal (2011)
N III	$^2P_{1/2}^o$	$^2P_{3/2}^o$	179.4	0.0222	Liang et al. (2012)
S III	3P_0	3P_1	298.7	0.0370	Hudson et al. (2012)
O III	3P_0	3P_2	306.2	0.0380	Tayal & Zatsarinny (2017)
Ne III	3P_2	3P_1	642.9	0.0797	McLaughlin & Bell (2000)
Ne II	$^2P_{3/2}^o$	$^2P_{1/2}^o$	780.4	0.0968	Griffin et al. (2001)
S III	3P_0	3P_2	833.1	0.103	Hudson et al. (2012)
Ne III	3P_2	3P_0	920.6	0.114	McLaughlin & Bell (2000)
S III	3P_0	1D_2	11323	1.404	Hudson et al. (2012)
N II	3P_0	1D_2	15316	1.899	Tayal (2011)
O III	3P_0	1D_2	20273	2.513	Tayal & Zatsarinny (2017)
Ne III	3P_2	1D_2	25841	3.204	McLaughlin & Bell (2000)
O II	$^4S_{3/2}^o$	$^2D_{5/2}^o$	26811	3.324	Tayal (2007)
O II	$^4S_{3/2}^o$	$^2D_{3/2}^o$	26831	3.327	Tayal (2007)
S III	3P_0	1S_0	27161	3.367	Hudson et al. (2012)
N II	3P_0	1S_0	32689	4.053	Tayal (2011)
O II	$^4S_{3/2}^o$	$^2P_{3/2}^o$	40468	5.017	Tayal (2007)
O II	$^4S_{3/2}^o$	$^2P_{1/2}^o$	40470	5.017	Tayal (2007)
C II	$^2P_{1/2}^o$	$^4P_{1/2}$	43003	5.332	Liang et al. (2012)
C II	$^2P_{1/2}^o$	$^4P_{3/2}$	43025	5.334	Liang et al. (2012)
C II	$^2P_{1/2}^o$	$^4P_{5/2}$	43054	5.334	Liang et al. (2012)
O III	3P_0	1S_0	43186	5.354	Tayal & Zatsarinny (2017)
C III	1S_0	$^3P_0^o$	52367	6.492	Aggarwal & Keenan (2015)
C III	1S_0	$^3P_1^o$	52391	6.495	Aggarwal & Keenan (2015)
C III	1S_0	$^3P_2^o$	52447	6.502	Aggarwal & Keenan (2015)
Ne III	3P_2	1S_0	55753	6.913	McLaughlin & Bell (2000)
N III	$^2P_{1/2}^o$	$^4P_{1/2}$	57187	7.090	Liang et al. (2012)
N III	$^2P_{1/2}^o$	$^4P_{3/2}$	57247	7.098	Liang et al. (2012)
N III	$^2P_{1/2}^o$	$^4P_{5/2}$	57328	7.108	Liang et al. (2012)

where g_ℓ is the degeneracy of the lower level ℓ . The rate coefficient for inelastic scattering of an electron of energy $E_i > \Delta E_{u\ell}$ is

$$(\sigma v)_i^{(\text{inel.})} = \pi a_0^2 \frac{I_H}{E_i} \frac{\Omega_{\ell \rightarrow u}(E_i)}{g_\ell} \left(\frac{2E_i}{m_e} \right)^{1/2}. \quad (22)$$

The collision strengths $\Omega_{\ell \rightarrow u}(E)$ were obtained from the sources listed in Table 1. The resulting rate coefficients are shown in Figures 2 and 3. We used the energy-dependent cross sections when available, giving rate coefficients with sharp structure at resonances (e.g., resonances in rates for excitation of the 3P_1 and 3P_2 levels of O III in Figure 2a). When energy-dependent cross sections were not available, we used simple fits that reproduced the calculated temperature-dependence of

Table 2: Test Cases

input parameter	H II region	Planetary Nebula
T_\star (K)	3.5×10^4	1.0×10^5
n_e (cm^{-3})	1	1
n_e/n_{H}	1.1	1.1
$n(\text{C III})/n_{\text{H}}$	$0.5 \times 2.95 \times 10^{-4}$	$1.0 \times 2.95 \times 10^{-4}$
$n(\text{N II})/n_{\text{H}}$	$0.5 \times 7.41 \times 10^{-5}$	0
$n(\text{N III})/n_{\text{H}}$	$0.5 \times 7.41 \times 10^{-5}$	$1.0 \times 7.41 \times 10^{-5}$
$n(\text{O II})/n_{\text{H}}$	$0.4 \times 5.37 \times 10^{-4}$	0
$n(\text{O III})/n_{\text{H}}$	$0.4 \times 5.37 \times 10^{-4}$	$1.0 \times 5.37 \times 10^{-4}$
$n(\text{Ne II})/n_{\text{H}}$	$0.5 \times 9.33 \times 10^{-5}$	$0.5 \times 9.33 \times 10^{-5}$
$n(\text{Ne III})/n_{\text{H}}$	$0.5 \times 9.33 \times 10^{-5}$	$0.5 \times 9.33 \times 10^{-5}$
$n(\text{S III})/n_{\text{H}}$	$1.0 \times 1.45 \times 10^{-5}$	$1.0 \times 1.45 \times 10^{-5}$
E_{max} (eV)	25	75
$\langle E_{\text{pe}} \rangle$ (eV)	4.22	15.83
resulting T_e (K)	6869	11129

the thermal rate coefficients (e.g., excitation of S III $^3\text{P}_1$ and $^3\text{P}_2$ in Figure 3a).

We assume that the density is low enough that excited states created by collisional excitation decay by spontaneous emission of a photon before collisional deexcitation can occur. Thus, we neglect superelastic processes where excited states are depopulated by collisions, and assume that every ion is in the ground state before a scattering encounter. This maximizes the collisional cooling rate relative to the photoionization heating rate, with both then having the same scaling with density n_e , so that the equilibrium temperature is independent of n_e .

Our treatment allows for fine-structure transitions which may be smaller than our energy bin width δE . Let $k \equiv \text{nint}(\Delta E_{ul}/\delta E)$, where $\text{nint}(x)$ is the nearest integer. If $k = 0$ we take

$$C_{i-1,i} = n_X \frac{\Delta E_{ul}}{\delta E} \times (\sigma v)_i^{(\text{inel.})} \quad \text{for } i > 1 . \quad (23)$$

If $k \geq 1$ we take

$$C_{1,k+1} = n_X \frac{\Delta E_{ul}}{k\delta E} \times (\sigma v)_i^{(\text{inel.})} \quad (24)$$

$$C_{i-k-1,i} = n_X f \times (\sigma v)_i^{(\text{inel.})} \quad \text{if } i > k + 1 \quad (25)$$

$$C_{i-k,i} = n_X (1 - f) \times (\sigma v)_i^{(\text{inel.})} \quad \text{if } i > k + 1 , \quad (26)$$

where $f \equiv (\Delta E_{ul}/\delta E) - k$, and n_X is the number density of the ion X .

These C_{ji} give the correct rate of energy loss for electrons with energy E_i . For electrons in the lowest energy bin $i = 1$ we neglect inelastic energy loss. So long as $P_1 \ll 1$ this underestimation

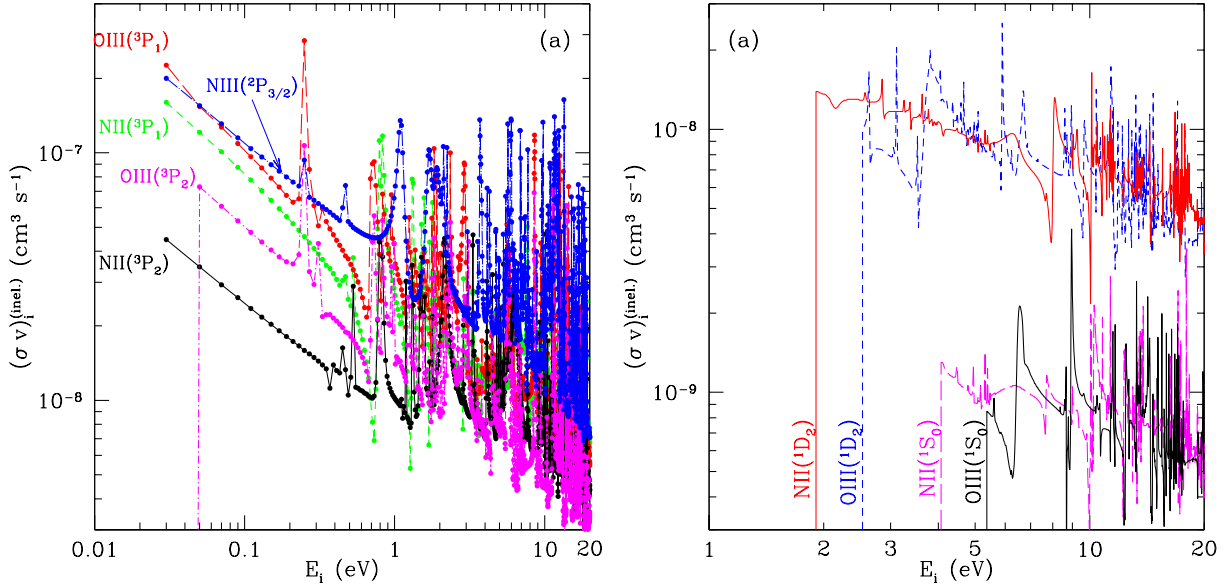


Fig. 2.— (a) Rate coefficients for fine structure excitation from the ground state 3P_0 to the excited fine structure levels of N II and O III as a function of electron energy E_i . Dots show the discrete energies E_j used in the calculations with $E_{\text{max}} = 25$ eV and $N = 1250$. The lowest energy $E_1 = 0.010$ eV is not shown, because energy loss is suppressed for electrons in this bin. (b) Rate coefficients for electronic excitation of N II and O III from the ground state 3P_0 . Cross sections are from Tayal (2011) and Tayal & Zatsarinsky (2017).

of collisional cooling is small. The final C_{ij} used in our calculations are obtained by summing over all of the cooling channels, using the ionic abundances n_X/n_H listed in Table 2. Relative to the protosolar abundances of Asplund et al. (2009) we take C to be 50% depleted, O to be 20% depleted, and N, Ne, and S to be undepleted. We assume the gas phase C and S to be doubly-ionized, and N, O, and Ne to be 50% singly-ionized, and 50% doubly-ionized. Our objective is only to have a reasonable representation of cooling processes and overall cooling rate, not to reproduce detailed ionization conditions at any particular location.

4. Steady-State Solutions for H II Region Conditions

4.1. Numerical Solutions with Suppression of Elastic Scattering

To examine the efficacy of electron-electron scattering, we consider a modified problem where all elastic scattering processes are suppressed by a factor γ . Thus we seek P_i satisfying the modified

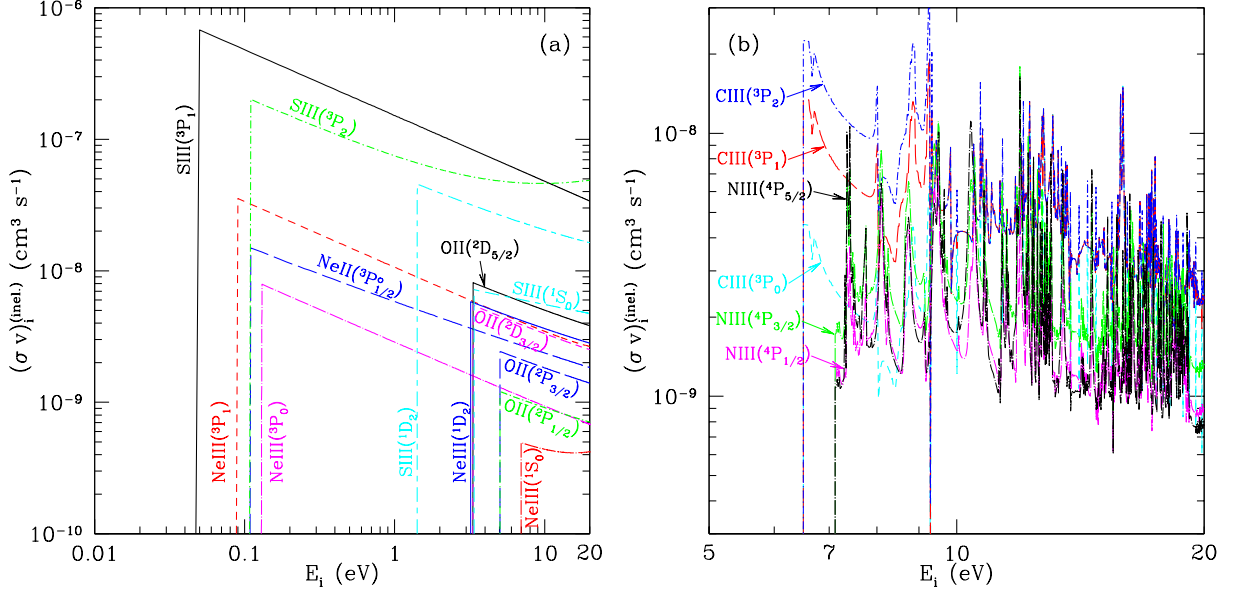


Fig. 3.— Rate coefficients for excitation of excited electronic states as a function of electron energy E_i (see text). (a) Analytic fits to rates for O II (Tayal 2007), Ne II (Griffin et al. 2001), Ne III (McLaughlin & Bell 2000), and S III (Hudson et al. 2012). (b) Rates for electronic excitation of C III (Aggarwal & Keenan 2015) and N III (Liang et al. 2012).

equations

$$\begin{aligned}
 0 = & \left(\sum_{j=1}^N R_j P_j \right) \phi_i - R_i P_i + \sum_{j=i+1}^N (B_{ij} + C_{ij}) P_j - \sum_{i=1}^{j-1} (B_{ji} + C_{ji}) P_i \\
 & + \gamma \left[\sum_{j=1}^{i-1} \sum_{k=i-j+1}^N A_{i-j,j,k} P_j P_k + \sum_{k=i+1}^N \sum_{j=1}^{N-(k-i)} A_{k-i,j,k} P_j P_k \right. \\
 & \left. - \sum_{j=1}^{N-i} \sum_{k=j+1}^N A_{j,i,k} P_i P_k - \sum_{j=1}^{i-1} \sum_{k=1}^{N-j} A_{j,k,i} P_k P_i \right]. \quad (27)
 \end{aligned}$$

For $\gamma = 1$ we recover the original physical problem, but by considering smaller values of γ we can illustrate the importance of elastic scattering compared to energy-changing processes.

Starting from an initial guess for the P_j , the steady-state solution P_j is found by iteration using the Fortran implementation of the Levenberg-Marquard algorithm from the minpack library (Garbow et al. 1980). Because elastic scattering is very fast compared to the energy-changing processes (photoionization, recombination, free-free emission, and collisional excitation) the Levenberg-Marquard algorithm, even using 64 bit arithmetic, only reaches an approximate steady-state. Therefore, after the Levenberg-Marquard algorithm has reached the limit of its numerical accuracy, we take the resulting P_i as a starting point and evolve forward in time. We have obtained accurate solutions to Eq. (27) for various values of γ . Figure 4 shows results for 5 values

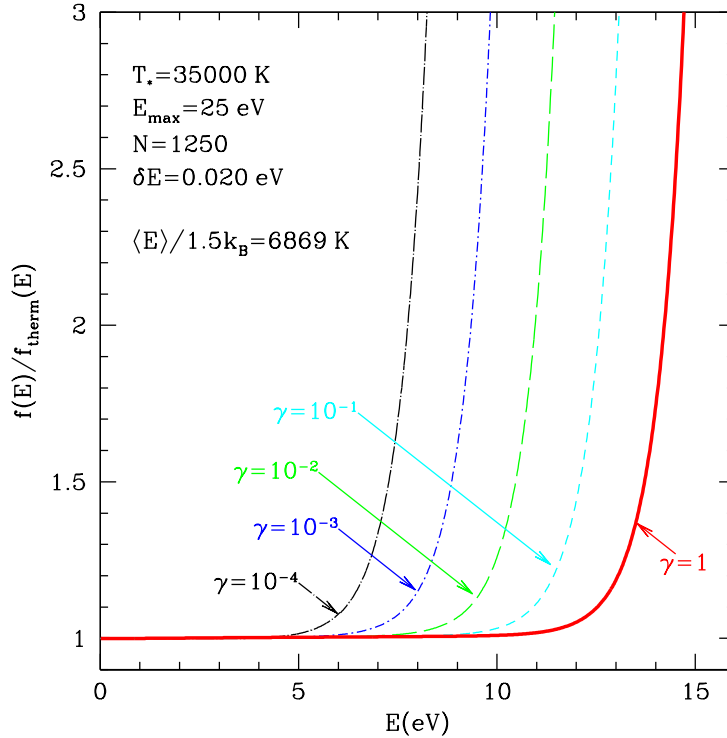


Fig. 4.— Solid curve: Steady-state electron distribution function relative to Maxwellian for the parameters in Table 2. The energy distribution is accurately described by a Maxwellian for $E \lesssim 13$ eV. Broken curves: distribution functions if elastic scattering is artificially suppressed by a factor γ . We see that even if elastic scattering is suppressed by a factor 10^{-4} , it is still able to maintain a Maxwellian distribution below 7 eV.

of γ , ranging from $\gamma = 10^{-4}$ to $\gamma = 1$.

The resulting statistical steady-state is in thermal equilibrium, with heating balancing cooling. The mean electron energy is $\langle E \rangle \equiv \sum P_j E_j$. We define the “temperature” to be

$$T \equiv \frac{\langle E \rangle}{1.5 k_B} . \quad (28)$$

In Figure 4 we show the electron energy distributions P_j relative to a Maxwellian distribution

$$\left(\frac{dP}{dE} \right)_{\text{MB}} = \frac{2}{\sqrt{\pi}} \frac{\sqrt{E}}{(k_B T)^{3/2}} e^{-E/k_B T} . \quad (29)$$

Even with elastic scattering suppressed by a factor $\gamma = 10^{-4}$, P_j accurately follows the Maxwell-Boltzmann distribution up to $E = 5$ eV, although there is a high energy tail that exceeds the Maxwell-Boltzmann distribution. As elastic scattering becomes stronger, it is able to maintain a thermal distribution of electron energies up to higher energies. For the physical case of $\gamma = 1$, the electrons are thermally-distributed up to ~ 13 eV, or $E/k_B T_{\text{eff}} \approx 20$.

Figure 5 shows the fraction of the electrons above energy E , as a function of E . The steady-state distribution is very close to a Maxwellian up to ~ 13 eV. Only a very small fraction –

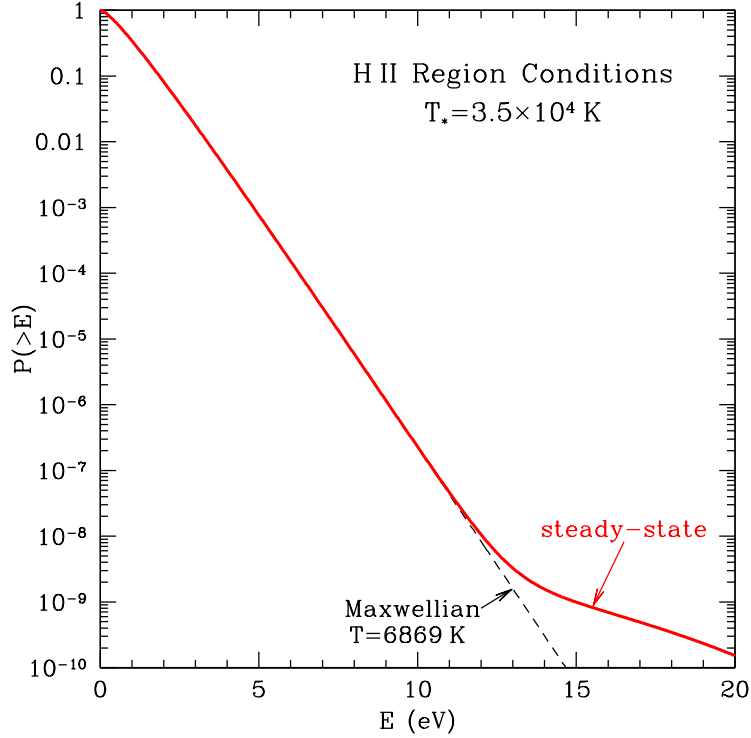


Fig. 5.— Fraction of electrons with energy $> E$, as a function of E , for the steady-state solution. Only $\sim 2 \times 10^{-9}$ of the electrons are in the nonthermal “tail” of the distribution at $E \gtrsim 13$ eV.

approximately 2×10^{-9} of the electrons are in the high energy tail maintained by steady injection of energetic photoelectrons.

4.2. κ -Distributions

The κ -distribution is (Vasyliunas 1968)

$$\left(\frac{dP}{dE}\right)_\kappa = \frac{2}{\sqrt{\pi}} \frac{1}{(\kappa - \frac{3}{2})^{3/2}} \frac{\Gamma(\kappa + 1)}{\Gamma(\kappa - \frac{1}{2})} \frac{\sqrt{E}}{(k_B T_U)^{3/2}} \left(1 + \frac{E}{(\kappa - \frac{3}{2})k_B T_U}\right)^{-(\kappa+1)}, \quad (30)$$

where $T_U \equiv (2/3)\langle E \rangle/k_B$ is the effective temperature, and κ is a dimensionless parameter. In the limit $\kappa \rightarrow \infty$ the κ -distribution converges to the Maxwell-Boltzmann distribution (29), but for $3/2 < \kappa < \infty$ the κ -distribution has relatively more electrons at high energies than the Maxwell-Boltzmann distribution with the same mean kinetic energy.

Vasyliunas (1968) used κ -distributions to describe electron energy distributions in the Earth’s magnetosphere measured by the OGO-1 and OGO-3 satellites, and since then κ -distributions have

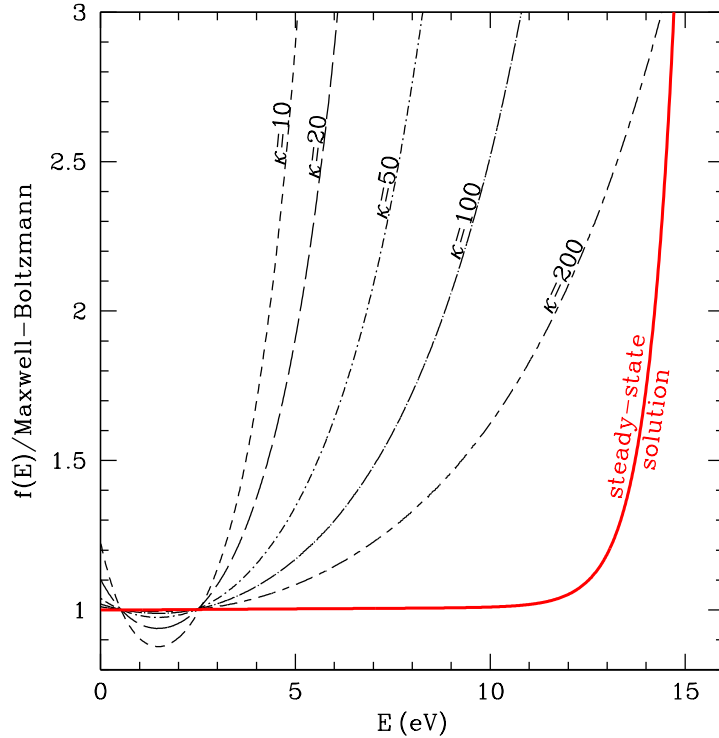


Fig. 6.— Steady-state electron energy distribution function (solid curve). Also shown are κ -distributions for $T_U = 6869$ K and $\kappa = 50, 100,$ and 200 . Even for $\kappa = 200$ the κ -distribution seriously overestimates the electron energy distribution between 5 and 14 eV. The Maxwellian distribution is an excellent approximation up to 13 eV.

often been used to describe “space plasmas”. Livadiotis & McComas (2011) discuss the theoretical basis for the κ -distribution as a non-equilibrium stationary state.

Nicholls et al. (2012) argue that the observed line ratios in H II regions are the result of κ -distributed electrons, with values of the κ parameter in the range $10 \lesssim \kappa \lesssim 20$. For planetary nebulae they found $\kappa \gtrsim 10$ from comparison of temperatures determined from [O III]4364/[O III]5009 with temperatures determined from the Balmer and Paschen breaks in the hydrogen recombination radiation.

In Figure 6 we compare our calculated steady-state solution for the electron energy distribution with κ -distributions. All cases have the same mean electron kinetic energy $\langle E \rangle = 0.8879$ eV (i.e., $T_U = 6869$ K). As in Figure 4, we show the energy distribution function divided by a Maxwellian distribution. Even for $\kappa = 200$, the κ -distribution substantially overestimates the fraction of electrons with energies in the 5–12 eV range. Up to 12 eV, the electron energy distribution is very accurately described by a Maxwellian, with factor-of-two departures present only above 14 eV.

5. Time-Dependent Solutions: Relaxation to the Stationary State

To illustrate the speed of relaxation to a near-Maxwellian distribution, we calculate the evolution of the electron energy distribution, starting from an initial distribution that is highly non-Maxwellian. We use the same physics: photoionization=recombination, recombination cross sections as in Section 3.2, and cooling by free-free emission and collisional excitation as in Sections 3.3 and 3.4.

Our objective here is only to show the speed of relaxation, so the initial conditions are arbitrary. While we include both cooling by free-free emission and line excitation, and photoionization balancing recombination, on the short time scales on which elastic scattering is able to thermalize the electron distribution, the energy of the plasma is nearly constant. For convenience, we choose an initial distribution with the same mean energy per particle as in the steady state solution with heating balancing cooling (corresponding to $T = 6869$ K), but we start with 90% of the electrons in a cold Maxwellian distribution with 50% of the total energy, and 10% of the electrons in a Maxwellian distribution with the remaining 50% of the energy. Thus the cooler Maxwellian has a temperature $T = 3816$ K, and the hotter Maxwellian has a temperature $T = 34345$ K.

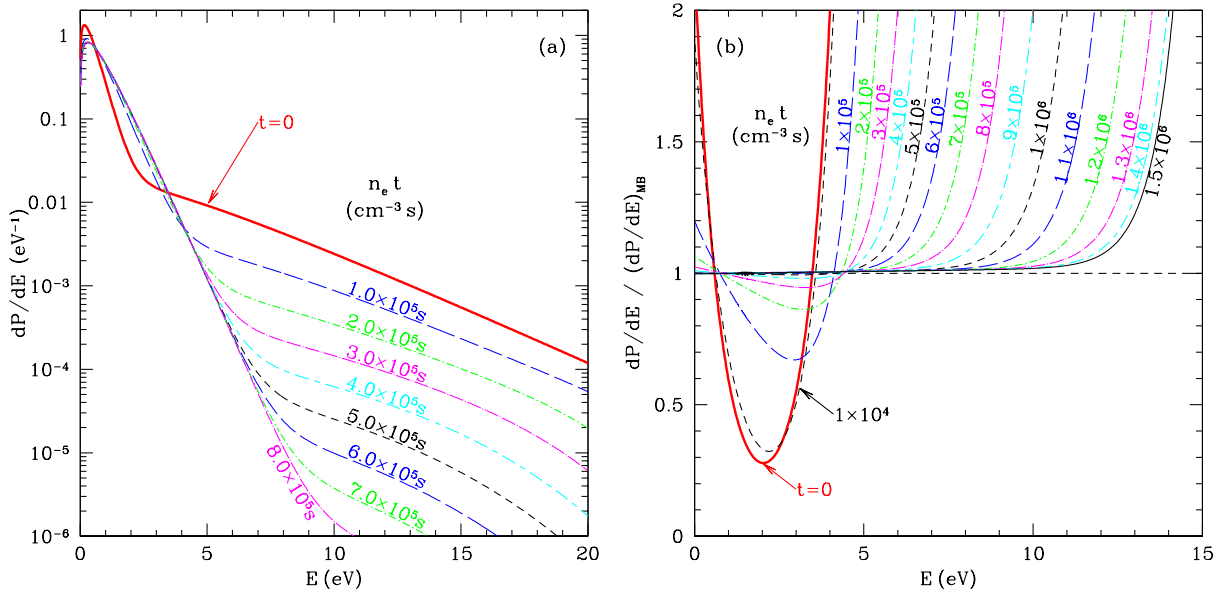


Fig. 7.— Relaxation toward a thermal distribution. (a) Electron energy distribution dP/dE at selected times. (b) Electron energy distribution relative to a Maxwellian, at selected times. For $E < 13$ eV, the distribution has relaxed to a Maxwellian after only 1.5×10^6 s for $n_e = 1 \text{ cm}^{-3}$.

Figure 7 shows evolution of the electron energy distribution, starting from the initial distribution at $t = 0$. The high energy tail relaxes on a time scale

$$\tau_{\text{relax}} \approx 10^5 \left(\frac{\text{cm}^{-3}}{n_e} \right) \text{sec} . \quad (31)$$

At the densities of the Orion nebula ($n_e \approx 3000 \text{ cm}^{-3}$), $\tau_{\text{relax}} \approx 30 \text{ s}$ – relaxation is extremely fast!

For this example, which begins with an extreme excess at high energies, the abundance of $\sim 10 \text{ eV}$ electrons drops by 4 orders of magnitude in $\sim 10^6 (\text{cm}^{-3}/n_e) \text{ s}$, and for $E \lesssim 13 \text{ eV}$ is accurately described by a Maxwellian after only $1.5 \times 10^6 (\text{cm}^{-3}/n_e) \text{ s}$. A time $\sim 10\tau_{\text{relax}}$ is required to reduce the extreme high energy tail by a factor $\sim 10^4$.

6. Planetary Nebulae

The nuclei of planetary nebulae have photospheric temperatures as high as $\sim 2 \times 10^5 \text{ K}$. Consequently, the plasma receives much more electron kinetic energy per photoionization than in the H II regions photoionized by O stars. The increased heating per photoionization results in higher gas temperatures.

Electron temperatures in the range 8000–20000 K have been estimated from the nebular and auroral lines of O III (Zhang et al. 2004). The line ratios in planetary nebulae often appear to be inconsistent with a single electron temperature, and the discrepancies have sometimes been attributed to κ -distributed electron energies (Zhang et al. 2016).

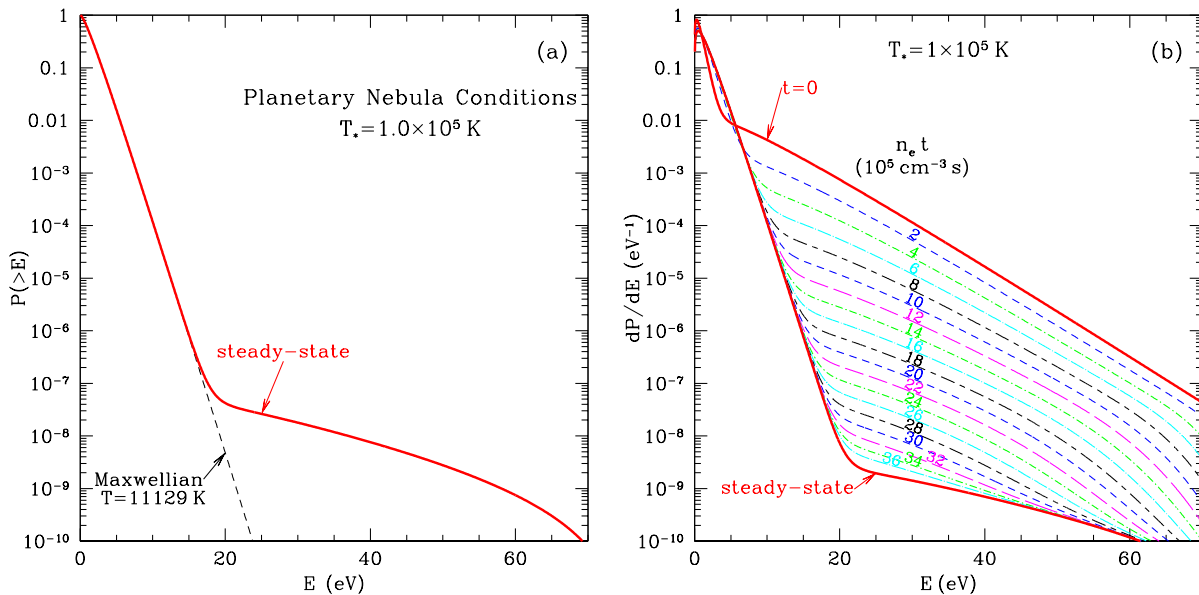


Fig. 8.— (a) Steady-state fraction of electrons with energy $> E$ as a function of E , for the average spectrum of photoelectrons for a stellar temperature $T_* = 10^5 \text{ K}$. Up to $E = 16 \text{ eV}$ the distribution is accurately described by a Maxwellian, but $\sim 5 \times 10^{-8}$ of the electrons are in a high-energy tail beginning at about $\sim 19 \text{ eV}$. (b) Time-dependent solutions, starting from a dual Maxwellian at $t = 0$ with 10% of the electrons containing 90% of the energy. The distribution relaxes toward the steady-state solution on a timescale $\sim 2 \times 10^5 (\text{cm}^{-3}/n_e) \text{ s}$.

Here we calculate the steady-state electron temperature in a plasma heated by the hard spectra present in planetary nebulae. As an example, we consider a stellar temperature $T_\star = 1.0 \times 10^5$ K, as for the central star of the Helix Nebula NGC 7291 (Napiwotzki 1999). We use the average spectrum of photoelectron energies from Eq. (11); for $T_\star = 10^5$ K, the mean energy of photoelectrons from H ionization is $\langle E_{pe} \rangle = 15.8$ eV.

Figure 8a shows the calculated cumulative steady-state electron energy distribution, compared to a Maxwellian with $T = 11129$ K. Nearly all of the electrons, up to $E \approx 16$ eV, are distributed following a Maxwellian distribution with $T = 11129$ K, but $\sim 3 \times 10^{-8}$ of the electrons are in a high energy tail extending to higher energies. The electrons in this tail were recently injected with energies $E > 20$ eV, and are in the process of slowing down to join the thermal distribution.

Figure 8b shows time-dependent relaxation toward the steady-state solution, for an initial distribution at $t = 0$ with the same mean energy per particle as in the steady-state solution, but with 90% of the energy contained in 10% of the particles (assumed to be in a Maxwellian distribution). Relaxation toward the steady-state solution takes place with a relaxation time

$$\tau_{\text{relax}} \approx 2 \times 10^5 \left(\frac{\text{cm}^{-3}}{n_e} \right) \text{ s} . \quad (32)$$

The relaxation time is longer than for H II region conditions (Eq. 31) because the mean energy per particle is larger by a factor $(11129/6869) = 1.62$, and the energy equipartition time for Coulomb scattering scales as $E^{1.5}$. For this illustrative example, a time $\sim 15\tau_{\text{relax}}$ is needed to become close to the steady state for $E \gtrsim 25$ eV, because the assumed initial conditions need to decay by a factor $\sim 10^6$ to reach the steady state. Nevertheless, the time $\sim 3 \times 10^6 (\text{cm}^{-3}/n_e)$ s is short compared to other time scales.

7. Summary

Local relaxation to a near-Maxwellian energy distribution is very rapid for the conditions in H II regions and planetary nebulae. There is no basis for using κ -distributions to describe the electrons in H II regions or planetary nebulae.

Given the speed of thermal relaxation ($\tau_{\text{relax}} \approx 30$ sec for Orion Nebula conditions), if observed line ratios and recombination spectra are found to be inconsistent with a single-temperature Maxwellian, this must be the result of the observed spectra summing emission from regions with different temperatures. Observations of real H II regions often include emission from an ionization front bounding the ionized gas, where photoionization can substantially exceed recombination, allowing heating rates to exceed the steady-state value. In addition to the ionization front at the outer boundary of the H II region, there may also be ionization fronts around dense neutral globules within the H II region that are undergoing “photoevaporation”. Such ionization fronts may locally have electron temperatures well above the temperatures in the bulk of the photoionized gas, where

photoionization is limited by the rate of radiative recombination, thus limiting the photoelectric heating.

The shorter time scales for photoionization in ionization fronts propagating into neutral gas will allow the electron population to have nonthermal “tails” that are larger than in the steady-state, but given that only $\sim 2 \times 10^{-9}$ of the electrons are in the nonthermal tail for steady-state photoionization (see Figure 5) in H II regions (or $\sim 5 \times 10^{-8}$ in planetary nebulae), it seems unlikely that the population of the nonthermal tail will be large enough to significantly affect spectra even in propagating photoionization fronts.

Thus observations of H II regions and planetary nebulae should be interpreted using a mixture of local temperatures (and ionization conditions) as originally proposed by Peimbert (1967). The electrons are locally well-approximated by Maxwellian distributions – κ -distributions do not apply.

We thank Gary Ferland for helpful suggestions that led to improvement of this paper. We are grateful to Kanti Aggarwal, Guiyun Liang, Brendan McLaughlin, Swaraj Tayal, and Oleg Zatsarinny for providing inelastic cross section data.

This work made use of the references provided in the CHIANTI atomic database (Dere et al. 1997; Del Zanna et al. 2015). This research was supported in part by NSF grant AST-1408723, and in part by NSF Research Fellowship DGE 1656466 to CDK.

REFERENCES

- Aggarwal, K. M., & Keenan, F. P. 2015, *MNRAS*, 450, 1151
- Asplund, M., Grevesse, N., Sauval, A. J., & Scott, P. 2009, *ARA&A*, 47, 481
- Binette, L., & Luridiana, V. 2000, *Rev. Mexicana Astron. Astrofis.*, 36, 43
- Binette, L., Matadamas, R., Hägele, G. F., et al. 2012, *A&A*, 547, A29
- Del Zanna, G., Dere, K. P., Young, P. R., Landi, E., & Mason, H. E. 2015, *A&A*, 582, A56
- Dere, K. P., Landi, E., Mason, H. E., Monsignori Fossi, B. C., & Young, P. R. 1997, *A&AS*, 125, 149
- Dopita, M. A., Sutherland, R. S., Nicholls, D. C., Kewley, L. J., & Vogt, F. P. A. 2013, *ApJS*, 208, 10
- Draine, B. T. 2011, *Physics of the Interstellar and Intergalactic Medium* (Princeton, NJ: Princeton Univ. Press)
- Esteban, C. 2002, in *Revista Mexicana de Astronomia y Astrofisica Conference Series*, Vol. 12, Ionized Gaseous Nebulae, ed. W. J. Henney, J. Franco, & M. Martos, 56

- Ferland, G. J., Henney, W. J., O'Dell, C. R., & Peimbert, M. 2016, *Rev. Mexicana Astron. Astrofis.*, 52, 261
- Garbow, B. S., Hillstrom, K. E., & Moré, J. J. 1980, minpack project, Argonne National Laboratory, <http://www.netlib.org/minpack>
- Giammanco, C., & Beckman, J. E. 2005, *A&A*, 437, L11
- Griffin, D. C., Mitnik, D. M., & Badnell, N. R. 2001, *J. Phys. B*, 34, 4401
- Gruenwald, R., & Viegas, S. M. 1995, *A&A*, 303, 535
- Hudson, C. E., Ramsbottom, C. A., & Scott, M. P. 2012, *ApJ*, 750, 65
- Kingdon, J. B., & Ferland, G. J. 1995, *ApJ*, 450, 691
- Kingdon, J. B., & Ferland, G. J. 1998, *ApJ*, 506, 323
- Landau, L. D., & Lifshitz, E. M. 1976, *Mechanics* (Oxford: Pergamon Press)
- Liang, G. Y., Badnell, N. R., & Zhao, G. 2012, *A&A*, 547, A87
- Liu, X.-W., & Danziger, J. 1993, *MNRAS*, 263, 256
- Livadiotis, G., & McComas, D. J. 2011, *ApJ*, 741, 88
- Louise, R., & Monnet, G. 1969, *A&A*, 3, 270
- McLaughlin, B. M., & Bell, K. L. 2000, *Journal of Physics B Atomic Molecular Physics*, 33, 597
- Mendoza, C., & Bautista, M. A. 2014, *ApJ*, 785, 91
- Napiwotzki, R. 1999, *A&A*, 350, 101
- Nicholls, D. C., Dopita, M. A., & Sutherland, R. S. 2012, *ApJ*, 752, 148
- Nicholls, D. C., Dopita, M. A., Sutherland, R. S., Kewley, L. J., & Palay, E. 2013, *ApJS*, 207, 21
- O'Dell, C. R. 2001, *PASP*, 113, 29
- O'Dell, C. R., Peimbert, M., & Peimbert, A. 2003, *AJ*, 125, 2590
- Oliveira, V. A., Copetti, M. V. F., & Krabbe, A. C. 2008, *A&A*, 492, 463
- Peimbert, M. 1967, *ApJ*, 150, 825
- Perez, E. 1997, *MNRAS*, 290, 465
- Pierrard, V., & Lazar, M. 2010, *Sol. Phys.*, 267, 153

- Spitzer, L. 1968, Diffuse matter in space (New York: Interscience)
- Spitzer, L., Jr. 1941, ApJ, 93, 369
- Tayal, S. S. 2007, ApJS, 171, 331
- Tayal, S. S. 2011, ApJS, 195, 12
- Tayal, S. S., & Zatsarinny, O. 2017, ApJ, 850, 147
- Vasyliunas, V. M. 1968, J. Geophys. Res., 73, 2839
- Zhang, Y., Ercolano, B., & Liu, X.-W. 2007, A&A, 464, 631
- Zhang, Y., Liu, X., Wesson, R., et al. 2004, MNRAS, 351, 935
- Zhang, Y., Liu, X.-W., & Zhang, B. 2014, ApJ, 780, 93
- Zhang, Y., Zhang, B., & Liu, X.-W. 2016, ApJ, 817, 68

A. Electron-Electron Scattering

The electron-electron scattering problem is straightforward kinematics plus Rutherford scattering. Because the algebra is somewhat involved, we collect the results here.

Let \mathbf{v}_j and \mathbf{v}_k be the electron velocities before scattering, with $\mathbf{v}_j \cdot \mathbf{v}_k = v_j v_k \cos \Theta$. After scattering the velocities are \mathbf{v}'_j and \mathbf{v}'_k . The relative speed is

$$|\mathbf{v}_j - \mathbf{v}_k| = \left(\frac{2}{m}\right)^{1/2} \left[E_j + E_k - 2\sqrt{E_j E_k} \cos \Theta \right]^{1/2}. \quad (\text{A1})$$

The energy gain by particle j is

$$\Delta E_j = \alpha \sqrt{E_j E_k} \quad (\text{A2})$$

$$\alpha(\theta) = \beta(1 - \cos \theta) + \gamma \sin \theta \quad (\text{A3})$$

$$\beta \equiv \frac{E_k - E_j}{2\sqrt{E_j E_k}} \quad (\text{A4})$$

$$\gamma \equiv \sin \Theta \cos \phi, \quad (\text{A5})$$

where θ is the scattering angle in the center-of-mass frame, and $0 \leq \phi \leq 2\pi$ is the angle between the $\mathbf{v}_j - \mathbf{v}_k$ plane and the $\mathbf{v}'_j - \mathbf{v}'_k$ plane.

B. A_{ijk} for $i > 1$ and $k > j$

For an electron with initial energy E_j , scattering off electrons with energy E_k , the rate of energy transfer in scattering events with $\Delta E \equiv E'_j - E_j$ satisfying

$$\Delta E \in \left[\left(i - \frac{1}{2} \right), \left(i + \frac{1}{2} \right) \right] \delta E \quad (\text{B1})$$

is

$$i\delta E \times n_k A_{ijk} = n_k \int_0^\pi \frac{\sin \Theta d\Theta}{2} |\mathbf{v}_j - \mathbf{v}_k| \int'' d\Omega \Delta E \frac{d\sigma}{d\Omega}, \quad (\text{B2})$$

where n_k is the number density of electrons with energy E_k , and \int'' is limited to (θ, ϕ) such that Eq. (B1) is satisfied. Let

$$Q_{lu}(E_j, E_k, \Theta, \phi) \equiv \int' d\theta \sin \theta \Delta E_j \frac{d\sigma(\theta)}{d\Omega}, \quad (\text{B3})$$

where \int' is limited to θ values such that Eq. (B1) is satisfied, i.e.,

$$\alpha(\theta) \in \left[\left(i - \frac{1}{2} \right), \left(i + \frac{1}{2} \right) \right] \frac{\delta E}{\sqrt{E_j E_k}} \quad \text{for } i > 1. \quad (\text{B4})$$

Then

$$A_{ijk} = \frac{1}{2i\delta E} \int_0^\pi \sin \Theta d\Theta |\mathbf{v}_j - \mathbf{v}_k| \int' d\phi Q_{lu}(E_j, E_k, \Theta, \phi). \quad (\text{B5})$$

For Rutherford scattering, we have

$$Q_{lu}(E_j, E_k, \Theta, \phi) = \sqrt{E_j E_k} \left(\frac{e^2}{4E_{\text{CM}}} \right)^2 \int' d\theta \frac{\sin \theta}{\sin^4(\theta/2)} [\beta(1 - \cos \theta) + \gamma \sin \theta]. \quad (\text{B6})$$

C. A_{ijk} for $i = 1$ and $k > j$

Because of the importance of weak, small-angle scattering, evaluation of A_{ijk} requires special treatment when $i = 1$. Because we want all of the weak energy transfer events included, we include all events with

$$\Delta E \in \left[0, \frac{3}{2} \right] \delta E, \quad (\text{C1})$$

or

$$\alpha(\theta) \in \left[0, \frac{3}{2} \right] \frac{\delta E}{\sqrt{E_j E_k}} \quad \text{for } i = 1. \quad (\text{C2})$$

D. A_{ijk} for $k \leq j$ from Detailed Balance

The principle of microscopic reversibility requires that

$$g_j g_k A_{ijk} = g_{k-i} g_{j+i} A_{i,k-i,j+i} , \quad (\text{D1})$$

where g_j is the “degeneracy” of energy bin j . Each of our “bins” includes a range of energies. g_j is proportional to the number of quantum states within the energy interval, with

$$g_j \propto \int' v^2 dv , \quad (\text{D2})$$

where \int' extends over kinetic energies in $[E_j - \delta E/2, E_j + \delta E/2]$. Thus

$$g_j \propto \int' E^{1/2} dE = \frac{2}{3} \left[\left(E_j + \frac{\delta E}{2} \right)^{3/2} - \left(E_j - \frac{\delta E}{2} \right)^{3/2} \right] \quad (\text{D3})$$

$$\propto E_j^{1/2} \delta E \left[1 - \frac{1}{96} \left(\frac{\delta E}{E_j} \right)^2 + O \left(\frac{\delta E}{E_j} \right)^4 \right] . \quad (\text{D4})$$

Thus, to leading order in $\delta E/E_j$,

$$A_{ijk} \approx \frac{E_{j+i}^{1/2} E_{k-i}^{1/2}}{E_j^{1/2} E_k^{1/2}} A_{i,k-i,j+i} = \sqrt{\frac{(j+i-\frac{1}{2})(k-i-\frac{1}{2})}{(j-\frac{1}{2})(k-\frac{1}{2})}} A_{i,k-i,j+i} . \quad (\text{D5})$$

Once we compute all the A_{ijk} for $j < k$, we can obtain the remaining A_{ijk} using Eq. (D5).